Semiempirical tight-binding interatomic potentials based on the Hubbard model

Qian Xie*
Max-Planck-Institut für Physik komplexer Systeme, Bayreuther Strasse 40, Dresden, D-01187, Germany

Peng Chen
Advanced Materials and Process Engineering Laboratory, Department of Physics, University of British Columbia 2355 East Mall, Vancouver, V6T 1Z1, Canada

(Received 17 December 1996; revised manuscript received 14 March 1997)

By use of the perturbation method for the Hubbard model, we discuss the contribution of the interatomic electron correlations to the cohesive energy in terms of the bond-order potential. With the first-order approximation for the bond order, we present a semiempirical tight-binding model for the interatomic potential. Based on this model, the influence of the on-site Coulomb interaction on materials properties such as phase stability, Cauchy pressure, and elastic anisotropy ratio is studied. It is shown that although it is a pair-functional one, the present model can describe very well the elastic properties and phase stabilities of the bcc transition metals without resorting to angular bonding or spline-function modeling. The model is also applied to calculating the epitaxial Bain paths. The results show that V, Nb, Cr, and W have a metastable tetragonal phase while Ta, Mo, and Fe do not. The vacancy-formation energies and surface tensions calculated with the suggested parameters for V, Nb, Ta, and Fe are reasonable, while those for Cr, Mo, and W are not correct. [S0163-1829(97)02534-4]

I. INTRODUCTION

The extensive interest in atomistic simulation for materials has resulted in the need to develop robust interatomic potentials. The past decade saw the development of different potentials, such as the widely used embedded-atom method (EAM) for the Cu and Ni columns of the transition metals[1] (or its equivalent, the glue model[2]) and Tersoff's empirical many-body potential for Si.[3]

One path to the quantum-mechanical interatomic potentials is to derive them from the very beginning, namely, from the Hamiltonian. This has been well exemplified by the bond-order potential (BOP) of Pettifor, which is derived from the tight-binding (TB) Hamiltonian by using the Lanczos recursion algorithm and the Green's function theory.[4–6] It has been shown that both the EAM and the Tersoff potential are just to some extent the approximations of the BOP.[7] One remarkable success of the BOP is its ability to reveal the structural trend across the transition metals. However, electron correlations may turn out to be important for the structural stabilities of narrow band solids like the *d*-band transition metals. The role of *d*-*d* electron correlations on the cohesion of the transition metals has been discussed by Friedel and Sayers using a second-order perturbation approximation based on Gutzwiller's approximation.[8] It is shown that the correlation energy increases the cohesion and decreases the surface tension and the maximum effect occurs in the half-filled case. Also the electron correlations are important in predicting the ground-state properties of group-IV semiconductors.[9] The calculated result for the interatomic correlation energy for diamond based on the local ansatz is -2.52 eV per unit cell, amounting to about a quarter of the Hartree-Fock cohesive energy.

The first-order approximation of the BOP, namely, the second-moment approximation of the tight-binding model (TB-SMA), has been proposed by a number of authors.[10,11] In the TB-SMA, the cohesive energy is written as

$$E_{\mathrm{coh}}=\frac{1}{2}\sum_{i,j\neq i} V_{ij}(R_{ij})-\sum_{i}\sqrt{\sum_{j\neq i} h_{ij}^{2}(R_{ij})}, \qquad (1)$$

where h_{ij} are the hopping integrals, V_{ij} are the repulsive pair potentials added to avoid collapse, and R_{ij} are the distances between atoms i and j. The above model can exactly be derived provided that the density of state is of rectangular shape. It has been shown that Eq. (1) is able to describe very well the properties of the fcc transition metals and alloys with full or nearly full *d* bands.[12] However, there are some problems when it is used to model the bcc transition metals with half-filled or nearly-half-filled *d* bands. The calculated elastic anisotropy ratios are sometimes too large. Moreover, it usually tends to predict the close-packed lattice as the ground-state structure if the cutoff distance is reasonably long (so that the contribution of the atoms beyond the cutoff to the total energy can be reasonably smaller than the desired structural energy difference). This is a common problem for the pair-functional models.[13] There have been some attempts to attack these problems such as using a more flexible spline-function model[10,14] and considering contributions of low-order moments.[15] However, the spline-function potentials are short ranged, and the results of structural stabilities produced by them are sensitive to the unphysically imposed cutoff and hence quite arbitary. On the other hand, the low-order moments method goes beyond the pair-functional category and thus becomes rather time consuming when applied to molecular-dynamics simulation.

In this paper, we use a single-band BOP associated with the perturbation method for the Hubbard model to derive a semiempirical TB potential. Based on this model, we study the effect of electron correlations on the materials properties. We show that the present model, being a pair-functional one, can be used to give correct phase stabilities and elastic con-

stants for the bcc transition metals. Also it can be used to model the materials with negative Cauchy pressures. Moreover, it is applied to studying the Bain paths. It is found that only some bcc transition metals have a metastable tetragonal phase. On the other hand, the calculated vacancy-formation energies and surface tensions for Cr, Mo, and W are unfortunately not correct at all, in spite of the fact that those for the other metals are basically reasonable.

II. ELECTRON CORRELATIONS IN THE BOND-ORDER FORMALISM

To study the electron correlations, the single-band Hubbard Hamiltonian $\hat{H}=\hat{H}_{\rm TB}+\hat{H}_{\rm int}$ is employed, where $\hat{H}_{\rm TB}$ is the single-band TB Hamiltonian used in the BOP for the noninteracting electrons, $\hat{H}_{\rm int}=\Sigma_{i\sigma}(U_i/2)\hat{n}_{i\sigma}\hat{n}_{i\bar{\sigma}}$, with U_i denoting the on-site Coulomb repulsion, and $\hat{n}_{i\sigma}$ the number operator for the local state $|i\rangle$ with spin σ. In the case when U_i is small the total energy can be written in the second-order perturbation form[16]

$$E_{\rm total}=E_0+\langle 0|\hat{H}_{\rm int}|0\rangle+\sum_{f\neq 0}\frac{|\langle 0|\hat{H}_{\rm int}|f\rangle|^2}{E_0-E_f}, \tag{2}$$

where $|0\rangle$ and $|f\rangle$ are the ground and excited states for the noninteracting system, which can be written in terms of the Slater determinants constructed with one-electron wave functions, and E_0 and E_f are the eigenenergies for the ground and excited states, respectively.

The first-order perturbation energy is simply $E_1=(1/2)\Sigma_{i\sigma}U_i\langle\hat{n}_{i\sigma}\rangle\langle\hat{n}_{i\bar{\sigma}}\rangle$, where $\langle\hat{n}_{i\sigma}\rangle$ is the local electron number on site i with spin σ, which is given by $\langle\hat{n}_{i\sigma}\rangle=\int^{E_F}\rho_{i\sigma}(E)dE$, where $\rho_{i\sigma}(E)$ is the corresponding local density of states (LDOS) and E_F the Fermi energy. There are two types of second-order terms associated with the excitation of one or two electron-hole pairs. In the case of single electron-hole pair excitation, the perturbation energy $E_2^{(1)}=\langle 0|\hat{H}_{\rm int}|f^{(1)}\rangle$ can be written as

$$E_2^{(1)}=\sum_{ij,\sigma}U_iU_j\langle\hat{n}_{i\sigma}\rangle\langle\hat{n}_{j\bar{\sigma}}\rangle\int^{E_F}dE_m\int_{E_F}dE_p\frac{\rho_{ij}^{\sigma}(E_m)\rho_{ji}^{\sigma}(E_p)}{E_m-E_p}, \tag{3}$$

where $\rho_{ij}^{\sigma}(E)$ are the LDOS (if $i=j$) and the intersite density of states (if $i\neq j$), defined by

$$\rho_{ij}^{\sigma}(E)=-\frac{1}{\pi}\lim_{\eta\to 0}{\rm Im}G_{ij}^{\sigma}(E+i\eta), \tag{4}$$

where $G_{ij}(E)$ are the intersite Green's functions. If U_i and $\langle n_{i\bar{\sigma}}\rangle$ do not change from site to site and the bases for the one-particle ground and excited states are orthogonal to each other, then one will find $E_2^{(1)}=0$.[16] However, the interatomic part of $E_2^{(1)}$, which is exactly the negative of the intra-atomic part, should not be neglected when calculating materials properties like the phonon spectrum, since the contribution of $E_2^{(1)}$ to the dynamical matrix does not vanish. There are some other reasons which make Eq. (3) not vanish, such as the effect of intersite charge transfer due to the asymmetric distribution of atoms in the presence of defects. Because of these reasons, we shall not neglect this contribution in the following derivation.

In the case of double electron-hole pair excitation, the perturbation energy $E_2^{(2)}=\langle 0|\hat{H}_{\rm int}|f^{(2)}\rangle$ can be written as

$$E_2^{(2)}=\frac{1}{2}\sum_{ij,\sigma}U_iU_j\int^{E_F}dE_m\int^{E_F}dE_n\int_{E_F}dE_p\int_{E_F}dE_q \times\frac{\rho_{ij}^{\sigma}(E_m)\rho_{ij}^{\bar{\sigma}}(E_n)\rho_{ji}^{\sigma}(E_p)\rho_{ji}^{\bar{\sigma}}(E_q)}{E_m+E_n-E_p-E_q}. \tag{5}$$

As a reasonable approximation,[16] the denominators in Eqs. (3) and (5) are replaced by average values $-W_{ij}^{(1)}$ and $-W_{ij}^{(2)}$. Thus Eqs. (3) and (5) can be written as

$$E_2^{(1)}=-\sum_{ij,\sigma}\frac{U_iU_j}{W_{ij}^{(1)}}\langle\hat{n}_{i\sigma}\rangle\langle\hat{n}_{j\bar{\sigma}}\rangle\Theta_{ij}^{\sigma}(P_{ji}^{\sigma}-\Theta_{ji}^{\sigma}) \tag{6}$$

and

$$E_2^{(2)}=-\sum_{ij,\sigma}\frac{U_iU_j}{2W_{ij}^{(2)}}\Theta_{ij}^{\sigma}\Theta_{ij}^{\bar{\sigma}}(P_{ji}^{\sigma}-\Theta_{ji}^{\sigma})(P_{ji}^{\bar{\sigma}}-\Theta_{ji}^{\bar{\sigma}}), \tag{7}$$

with

$$P_{ij}^{\sigma}=\int^{E_U}\rho_{ij}^{\sigma}(E)dE, \tag{8}$$

$$\Theta_{ij}^{\sigma}=\int^{E_F}\rho_{ij}^{\sigma}(E)dE, \tag{9}$$

where E_U is the upper bound of the band, Θ_{ij}^{σ} is the bond order with spin σ, and P_{ij}^{σ} is the bond order with full band.

In this paper, magnetism is not considered; i.e., the local net spin $\langle\hat{n}_{i\sigma}\rangle-\langle\hat{n}_{i\bar{\sigma}}\rangle$ is assumed to be zero, or $\langle\hat{n}_{i\sigma}\rangle=\langle\hat{n}_{i\bar{\sigma}}\rangle=N_i/2$ (N_i is the on-site occupation number). If all the sites are assumed to be equivalent, then the intrasite correlation energy can be expressed by

$$E_{2,0}^{(1)}=-(2U^2/W_0^{(1)})(N/2)^3(1-N/2)$$

and

$$E_{2,0}^{(2)}=-(U^2/W_0^{(2)})(N/2)^2(1-N/2)^2.$$

These contributions, together with the term E_1, are not the interatomic parts which contribute to crystal binding (in this regard, we would like to point out that the treatment in Ref. 8 is problematical since the intrasite correlation terms contribute nothing to the *cohesive energy* of the system).

For the interatomic contributions, let us first observe what N_{ij} and Θ_{ij} ($i\neq j$) will be within the framework of the BOP. The bond order can be written as[4]

$$\Theta_{ij}=-\sum_{n=0}^{\infty}\chi_{0n,n0}(E_F)\,\delta a_n^{\lambda}-\sum_{n=1}^{\infty}\chi_{0(n-1),n0}(E_F)2\,\delta b_n^{\lambda} \tag{10}$$

and similiarly P_{ij} can be written as

$$P_{ij}=-\sum_{n=0}^{\infty}\chi_{0n,n0}(E_U)\,\delta a_n^{\lambda}-\sum_{n=1}^{\infty}\chi_{0(n-1),n0}(E_U)2\,\delta b_n^{\lambda}, \tag{11}$$

where the response functions $\chi_{0m,n0}(\omega)$ are defined by

$$\chi_{0m,n0}(\omega)=\frac{1}{\pi}\lim_{\eta\to 0}\mathrm{Im}\int^{\omega}G_{0m}^{\lambda}(E+i\eta)G_{n0}^{\lambda}(E+i\eta)dE. \tag{12}$$

$G_{nm}^{\lambda}(E)$ are the Green's functions on the recursion basis, λ is the phase factor for the initial state of the Lanczos recursion $|\Psi_0^{\lambda}\rangle=(1/\sqrt{2})[|i\rangle+\exp(i\phi)|j\rangle]$, which is defined as $\lambda=\cos\phi$, and δa_n^{λ} and δb_n^{λ} are the derivatives of the recursion coefficients a_n^{λ} and b_n^{λ} with respect to the phase factor λ: $\delta a_n^{\lambda}=\partial a_n^{\lambda}/\partial\lambda$ and $\delta b_n^{\lambda}=\partial b_n^{\lambda}/\partial\lambda$.

If Pettifor's approximation is used, i.e., the recursion coefficients are taken to be the same, $a_n^{\lambda}=0$, $b_n^{\lambda}=b=-\sqrt{[\Sigma_{k\neq i}h_{ki}^2+\Sigma_{k\neq j}h_{kj}^2]/2}$, then the reduced response functions $\hat{\chi}_p=|b|\chi_p(p=m+n+2)$ will be[4] $\hat{\chi}_p(\omega)=\sin[(p-1)\theta_\omega]/[(p-1)\pi]-\sin[(p+1)\theta_\omega]/[(p+1)\pi]$, with $\cos\theta_\omega=\omega/2b$. In this approximation, the LDOS is of a semielliptic shape, with the upper bound equal to $-2b$. This corresponds to $\theta_U=\pi$. Therefore, $\hat{\chi}_p(E_U)=0$ and $P_{ij}=0$. Thus we have the interatomic perturbation energies

$$E_{\mathrm{inter}}=\sum_{i,j\neq i}\left[\frac{U_iU_jN_iN_j}{2W_{ij}^{(1)}}\Theta_{ij}^2-\frac{U_iU_j}{W_{ij}^{(2)}}\Theta_{ij}^4\right], \tag{13}$$

where the spin degeneracy has been considered. The above equation says that the contribution of electron correlations to the binding energy is a *nonlinear* function of the bond order (while the single-electron contribution scales linearly with the bond order).

III. SEMIEMPIRICAL TIGHT-BINDING INTERATOMIC POTENTIAL

In this section, we simplify the bond order by taking only the first-order term (i.e., the second-moment term) and write it as

$$\Theta_{ij}=-\frac{h(R_{ij})}{\sqrt{\sum_{k\neq i}h^2(R_{ik})}}, \tag{14}$$

where the prefactor of the first-order electronic response function has been dropped (actually it is this prefactor that says the correlation effect reaches maximum in the half-filled case). Equation (14) is exact for a hydrogen dimer. Considering the physical restriction that the lattice sum of the interatomic perturbation energy should converge when the crystal lattice is expanded to the atomic limit, we find that $W_{ij}^{(1)}$ and $W_{ij}^{(2)}$ should increase with respect to the increasing of the interatomic distance. For simplicity, they are assumed as follows: $U_iU_jN_iN_j/W_{ij}^{(1)}\propto h_{ij}$ and $U_iU_j/W_{ij}^{(2)}\propto h_{ij}$. By adding these two terms to the cohesive energy equation of the BOP, $E_{\mathrm{coh}}=(1/2)\Sigma_{i,j\neq i}V(R_{ij})+\Sigma_{i,j\neq i}h(R_{ij})\Theta_{ij}$ [within the first-order approximation it is, namely, Eq. (1)], we have the following expression for the binding energy per atom (for a perfect crystal):

$$E=\frac{1}{2}\sum_{i\neq 0}V(R_i)-\sqrt{\sum_{i\neq 0}g(R_i)}+U_1\sum_{i\neq 0}g^{3/2}(R_i)\Big/\sum_{i\neq 0}g(R_i)-U_2\sum_{i\neq 0}g^{5/2}(R_i)\Big/\left[\sum_{i\neq 0}g(R_i)\right]^2, \tag{15}$$

where R_i is the distance of atom i to the central atom, $g(r)=h^2(r)$, and U_1, U_2 are two dimensionless constants related to the on-site Coulomb repulsion of the Hubbard model. Equation (15) is the *central* point of this paper. The first two terms in Eq. (15) are the conventional TB-SMA. The remaining two terms are due to the Hubbard model, and will be referred to as U terms throughout this paper.

The contribution of the electron correlations to the cohesive energy should increase when enlarging the interatomic spacing or lattice constant (because localization becomes more significant).[9] Equation (15) shows this tendency—the ratio of the electron-correlation term (U_2 term) to the second-moment term, $U_2\Sigma_{i\neq 0}g^{5/2}(R_i)/[\Sigma_{i\neq 0}g(R_i)]^{5/2}$, increases when the lattice constant is increased.

According to the classification of Carlsson,[13] Eq. (15) is a pair-functional model. The pair-functional potentials are much simpler than the angularly dependent potentials for molecular-dynamics simulations. However, at least three problems hinder the application of the conventional pair-functional potentials like the EAM or TB-SMA. The first one is that they usually tend to predict the most close-packed lattice to be the ground-state structure.[13] The second one is that they impose positive Cauchy pressure (because the second derivative of the embedding function or second moment is always positive). The third one is that they usually give very wrong elastic constants for materials with low elastic anisotropy ratios. These problems are crucial in the field of computer simulation for crystal growth, because first in order to predict which structure can be grown on the substrate we need a reliable interaction model which is capable of reproducing the correct bulk properties, and second, the physically feasible structure of strained layers is related to the phase stabilities and elastic constants.

IV. INFLUENCE OF U TERMS ON MATERIAL PROPERTIES

In this section, we study the influence of the Coulomb parameters U_1 and U_2 on the physical properties of materials by using analytical modeling so that the results can be more explicit. For convenience, we assume that $g(r)$ and $V(r)$ are power-law functions:

$$V(r)=V_e\left(\frac{R_{1e}}{r}\right)^{\alpha}, \tag{16}$$

$$g(r)=g_e\left(\frac{R_{1e}}{r}\right)^{\beta}, \tag{17}$$

where R_{1e} is the equilibrium nearest-neighbor distance, and V_e, g_e, α, and β are parameters. The lattice sums

$$\Phi(R_1)=\sum_{m=1}^{\infty} w_m V(p_m R_1),$$

$$\Gamma(R_1)=\sum_{m=1}^{\infty} w_m g(p_m R_1), \quad J(R_1)=\sum_{m=1}^{\infty} w_m g^{3/2}(p_m R_1),$$

and

$$K(R_1)=\sum_{m=1}^{\infty} w_m g^{5/2}(p_m R_1)$$

(where w_m are the numbers of atoms on the mth shell with radius $p_m R_1$) are

$$\Phi(R_1)=S(\alpha)V_e(R_{1e}/R_1)^{\alpha}, \quad \Gamma(R_1)=S(\beta)g_e(R_{1e}/R_1)^{\beta},$$

$$J(R_1)=S(3\beta/2)g_e^{3/2}(R_{1e}/R_1)^{3\beta/2},$$

and

$$K(R_1)=S(5\beta/2)g_e^{5/2}(R_{1e}/R_1)^{5\beta/2},$$

where

$$S(x)=\sum_{m=1}^{\infty} w_m/p_m^x .$$

We choose the following properties which reflect the extent of how the interatomic potential deviates from the TB-SMA.

A. Phase stability

In the present model, the binding energy as a function of the nearest-neighbor distance R_1 is written as

$$E_{\mathrm{coh}}=\frac{1}{2}S(\alpha)V_e\left(\frac{R_{1e}}{R_1}\right)^{\alpha}-\sqrt{g_e}X(\beta)\left(\frac{R_{1e}}{R_1}\right)^{\beta/2}, \qquad (18)$$

where

$$X(\beta)=\sqrt{S(\beta)}-U_1\frac{S(3\beta/2)}{S(\beta)}+U_2\frac{S(5\beta/2)}{S^2(\beta)}. \qquad (19)$$

One can see from the above equation that the U terms improve the flexibility of the mininum energies with respect to structures.

B. Cauchy pressure

The elastic constants consist of the contributions of three terms: $C_{\mu\nu}=C_{\mu\nu}^{\mathrm{SMA}}+\delta C_{\mu\nu}+\delta^2 C_{\mu\nu}$, where $C_{\mu\nu}^{\mathrm{SMA}}$ are contributed by the first two terms of Eq. (15), and $\delta C_{\mu\nu}$ and $\delta^2 C_{\mu\nu}$ are contributed by the other two terms, respectively (see the Appendix for the expressions). The Cauchy pressure can be expressed by

$$\Omega(C_{12}-C_{44})=\frac{\beta^2\sqrt{g_e}}{9}\left[\frac{\sqrt{S(\beta)}}{4}-U_1\frac{S(3\beta/2)}{S(\beta)}+U_2\frac{4S(5\beta/2)}{S^2(\beta)}\right]. \qquad (20)$$

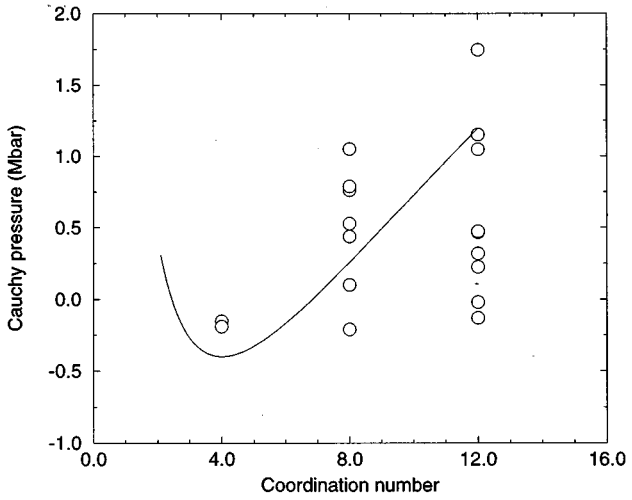

FIG. 1. Cauchy pressure $C_{12}-C_{44}$ vs coordination number z for the cubic structures diamond, bcc, and fcc. The circles are experimental data, taken from Simmons and Wang (Ref. 17). The curve is the fitting result with $U_1=0.80$, $U_2=0.25$.

Equation (20) shows that the present model is able to describe the materials with negative Cauchy pressures. If the nearest-neighbor approximation (NNA) is used, i.e., $S(x)=z$, then $\Omega(C_{12}-C_{44})=(\beta^2\sqrt{g_e}/9)(\sqrt{z}/4+4U_2/z-U_1)$, and the Cauchy pressure will change from negative to positive at a certain coordination number (Fig. 1). This is consistent with the fact that covalent solids with diamond structure ($z=4$) have negative Cauchy pressures while most of the transition metals ($z=8$ for bcc and $z=12$ for fcc) have positive ones.

C. Anisotropy ratio

The anisotropy ratio for the elastic constants Q refers to the ratio of the rhombohedral shear modulus C_{44} and the tetragonal shear modulus $C'=(C_{11}-C_{12})/2$. For bcc, with a cutoff between second- and third-nearest-neighbor distances, Q can be expressed by

$$Q=\frac{8}{9}\frac{R_1^2V''_{\mathrm{eff}}(R_1)-R_1V'_{\mathrm{eff}}(R_1)}{R_2^2V''_{\mathrm{eff}}(R_2)-R_2V'_{\mathrm{eff}}(R_2)}. \qquad (21)$$

The effective pair potential for the present model is the combination of three Lennard-Jones-like functions:

$$V_{\mathrm{eff}}(r)=\left[V_e\left(\frac{R_{1e}}{r}\right)^{\alpha}-\frac{\sqrt{g_e}}{\sqrt{S(\beta)}}\left(\frac{R_{1e}}{r}\right)^{\beta}\right]+U_1\frac{\sqrt{g_e}}{S(\beta)}\left[\left(\frac{R_{1e}}{r}\right)^{3\beta/2}-\frac{S(3\beta/2)}{S(\beta)}\left(\frac{R_{1e}}{r}\right)^{\beta}\right]-U_2\frac{\sqrt{g_e}}{S^2(\beta)}\left[\left(\frac{R_{1e}}{r}\right)^{5\beta/2}-\frac{2S(5\beta/2)}{S(\beta)}\left(\frac{R_{1e}}{r}\right)^{\beta}\right]. \qquad (22)$$

The collision radii for the above three Lennard-Jones-like potentials are

$[\alpha V_e\sqrt{S(\beta)}/\beta\sqrt{g_e}]^{1/(\alpha-\beta)}R_{1e}$, $[3S(\beta)/2S(3\beta/2)]^{2/\beta}R_{1e}$,

and

$$[5S(\beta)/4S(5\beta/2)]^{2/3\beta}R_{1e},$$

respectively. The problem of the anisotropy ratio for the bcc transition metals lies in the fact that the difference between the curvatures for the effective pair potential at the first- and second-nearest-neighbor distances should not be too large. From Eq. (22), one can see this can be reached because the negative third term plays the role of reducing the curvature. Within the framework of the TB-SMA (or the EAM), it is rather difficult to use conventional functions like the exponential or power law to slow down the rapidly decaying behavior of the curvature for the effective pair potential, because the decaying parameters determined from experimental data are usually too large.

V. APPLICATIONS OF THE POTENTIALS

In this section, we shall apply the above model to study real materials. For real materials we have to determine the potential parameters at first. Usually a least-squares fitting procedure is used, but in this work we do not intend to spend too much effort on obtaining the optimal parameters. We just find some suitable parameters and demonstrate numerically the model capability.

A. Fitting procedure

In the above section we employ power-law functions to study the model capability in an analytical way. Numerically a disadvantage for the power-law functions is that they converge too slowly ($r^{-\alpha}>e^{-\alpha r}$). We found that whatever the other parameters α and β should satisfy the equality $\alpha\beta/2=9B\Omega/E_s$, if one wants to obtain correct ground-state properties (i.e., the lattice constant a_e, the cohesive energy E_s, and the bulk modulus B). If the hopping integral converges faster (β becomes greater), then the pair potential will converge slower (α smaller) and vice versa. Therefore, the long-range tails cannot be eliminated by increasing α or β. Of course, more long-range potentials will result in greater computational effort because a larger neighbor list is needed.

In this section, we use the lattice-inversion method[18–20] (LIM) based on the Möbius inversion transform in number theory[21,22] to simplify the fitting procedure for obtaining the model paramters from the experimental data. We suppose that the cohesive energy as a function of nearest-neighbor distance is given by the universal binding energy curve of Rose *et al.*,[23]

$$E(R_1)=-E_s\left[1+\alpha\left(\frac{R_1}{R_{1e}}-1\right)\right]\exp\left[-\alpha\left(\frac{R_1}{R_{1e}}-1\right)\right], \tag{23}$$

where $\alpha=\sqrt{9B\Omega/E_s}$, B is the bulk modulus, Ω the atomic volume, and E_s the sublimation energy. We have the lattice summations of the square hopping integral and pair potential,

$$\sum_{m=1}^{\infty} w_m g(p_m R_1)=\Gamma(R_1), \tag{24}$$

TABLE I. Input experimental data and suggested parameters for the bcc transition metals. The lattice constants are in Å, the cohesive energies are in eV, the bulk moduli [which are obtained from experimental data by using $B=(C_{11}+2C_{12})/3$] are in 10^{11} N/m^2, U_1, U_2, β are dimensionless, and Γ_e are in eV^2.

Element	a_e	E_s	B	β	Γ_e	U_1	U_2
V	3.03[a]	5.31[a]	1.55[b]	6.5	150	3.5	9.1
Nb	3.30[a]	7.57[a]	1.71[b]	6.2	300	2.9	8.1
Ta	3.30[a]	8.10[a]	1.96[b]	5.7	300	3.5	10.0
Cr	2.88[a]	4.10[a]	1.90[b]	6.0	200	10.0	28.0
Mo	3.15[a]	6.82[a]	2.63[b]	8.0	100	11.5	30.0
W	3.16[a]	8.90[a]	3.10[b]	6.0	100	16.4	50.0
Fe	2.87[a]	4.28[a]	1.08[b]	6.0	100	3.7	8.5

[a]Reference 24.
[b]Reference 17.

$$\sum_{m=1}^{\infty} w_m V(p_m R_1)=\Phi(R_1), \tag{25}$$

where

$$(1/2)\Phi(R_1)=E(R_1)+\sqrt{\Gamma(R_1)}-U_1J(R_1)/\Gamma(R_1)+U_2K(R_1)/\Gamma^2(R_1). \tag{26}$$

And similiar to Ref. 18, $\Gamma(R_1)$ is assumed to be an exponential function:

$$\Gamma(R_1)=\Gamma_e\exp\left[-\beta\left(\frac{R_1}{R_{1e}}-1\right)\right]. \tag{27}$$

By using the LIM, $g(r)$ and $V(r)$ can be inverted from Eqs. (24) and (25):

$$g(r)=\sum_{m=1}^{\infty}\mu_m\Gamma(p_m r), \tag{28}$$

$$V(r)=\sum_{m=1}^{\infty}\mu_m\Phi(p_m r), \tag{29}$$

where μ_m are the Möbius inversion coefficients for crystal lattices. The pair potential and hopping integral defined above decay much faster (exponentially) than the power-law functions. Compared with the conventional fitting procedure, the inversion scheme skips searching for the optimal parameters for the pair potential and correct ground-state properties can be guaranteed.

The input experimental data for the universal equation of binding energy and suggested parameters are listed in Table I. The inverted results for the square hopping integrals and pair potentials for the bcc transition metals are shown in Fig. 2. The pair potentials have attraction wells (especially for Cr, Mo, and W).

B. Phase stabilities and elastic constants

Instead of C_{11}, C_{12}, and C_{44}, we calculate C', C_{44}, and B by distorting the crystal lattice with the corresponding strain matrices. The cutoff is carefully placed at the distance where the contribution of the hopping integral and pair po-

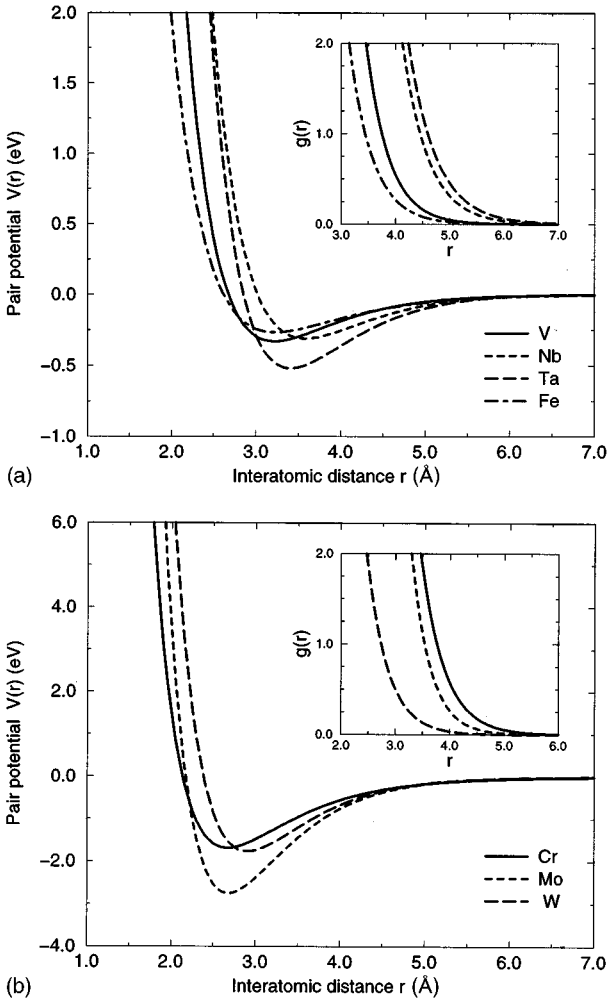

FIG. 2. Inverted pair potentials and square hopping integrals $g(r)$ (inset) as a function of interatomic distance. The unit for $g(r)$ is eV^2. (a) For V, Nb, Ta, and Fe; (b) for Cr, Mo, and W.

tential to the cohesive energy has been small enough to ensure the reliablity of the calculated results for the phase stabilities. The results for the phase stabilities and elastic constants are listed in Tables II and III. The bcc structure is calculated to be the most stable one over a range of coordination number from 4 (diamond) to 12 (fcc or hcp).

A simulation box of size $10\times10\times10$ (2000 atoms) is employed in the calculation of the vacancy-formation energies

TABLE II. Calculated energy differences for the bcc transition metals with the present model. The energies are in eV. The equilibrium nearest-neighbor distances for the corresponding structures (in Å) are also given.

Element	V	Nb	Ta	Cr	Mo	W	Fe
ΔE(sc-bcc)	0.854	0.831	1.195	1.947	3.720	2.980	0.749
r_{1e}(sc)	2.500	2.700	2.720	2.450	2.730	2.660	2.330
ΔE(fcc-bcc)	0.063	0.083	0.072	0.214	0.108	0.276	0.037
r_{1e}(fcc)	2.710	2.943	2.943	2.575	2.815	2.823	2.561
ΔE(hcp-bcc)	0.063	0.083	0.072	0.214	0.105	0.276	0.037
r_{1e}(hcp)	2.710	2.940	2.950	2.570	2.820	2.820	2.560
ΔE(diamond-bcc)	1.189	0.980	1.894	1.452	4.570	3.226	1.547
r_{1e}(diamond)	2.377	2.559	2.663	2.503	2.754	2.693	2.225

TABLE III. Calculated elastic constants, vacancy formation energies, and surface tensions for the bcc transition metals with the present model. The first row is the calculated results; the second is the experimental data. The elastic constants are in 10^{11} N/m^2, the anisotropic ratios $Q=2C_{44}/(C_{11}-C_{12})$ are dimensionless, γ_{100} are in mJ/m^2, and E_v are in eV. The data in parentheses are the relaxation energies for vacancy formation. Source of experimental data: Elastic constants are from Ref. 17; vacancy-formation energy of V is from Ref. 14; those for the others are from Ref. 10; surface energy for V is the theoretical result of Ref. 10, those for the others are experimental values from Ref. 10.

Element	C_{11}	C_{12}	C_{44}	Q	γ_{100}	E_v
V	2.141	1.256	0.427	0.96	4554	2.96(0.9)
	2.279	1.187	0.426	0.78	2600	2.10
Nb	2.243	1.442	0.261	0.65	3880	3.42(0.9)
	2.466	1.332	0.281	0.50	2300	2.04
Ta	2.508	1.687	0.849	2.07	5109	4.46(1.2)
	2.660	1.612	0.824	1.57	2780	2.90
Cr	3.919	0.881	1.042	0.69	16960	16.8(3.3)
	3.91	0.896	1.032	0.69	2200	1.20
Mo	4.318	1.788	1.157	0.92	11968	18.2(2.7)
	4.647	1.615	1.089	0.72	2200	2.24
W	5.179	2.067	1.630	1.05	21376	25.0(4.9)
	5.224	2.044	1.606	1.01	2800	3.15
Fe	1.558	0.845	0.783	2.20	6030	2.25(1.1)
	1.519	0.862	0.762	2.32	2200	1.79

E_v (periodic boundary condition applied to x,y,z directions) and (100) surface tensions γ_{100} (periodic boundary condition applied to x,y directions). The vacancy-formation energy is defined as the energy needed to move an atom from bulk to surface, rather than infinity. The unrelaxed results are presented in Table III. The relaxation energies for vacancy formation (computed by minimizing the energy with respect to atom positions; only the nearest neighbors around the vacancy are allowed to relax) are given in parentheses. The calculated results of E_v for V, Nb, Ta, and Fe are in reasonable agreement with the experimental data while those of unrelaxed surface tensions are higher than the experimental data (considering relaxation will surely help reduce the errors). Unfortunately, the calculated vacancy-formation energies and surface tensions for Cr, Mo, and W are much higher than the experimental data. It seems that there is some dependence related to bond breaking that correlates the elastic constants (without bond breaking) and the defect properties (with bond breaking). We failed in getting parameters which are able to reproduce both. While the defect properties may be reproduced with appropriate parameters, the results for the elastic constants may be as poor as those produced by the EAM. This severe disagreement seems to imply that the contributions from higher moments (i.e., directional bonding) should be considered.

C. Epitaxial Bain path

The martensitic transformation is a first-order displacive solid-solid phase transformation observed in a variety of materials. The Bain path refers to the path of intermediate tetragonal states between two phases connected to a martensi-

tic transformation, like the bcc and fcc. It has been pointed out in Ref. 25 that the study of Bain paths is instructive to the physics of crystal growth and thin films,[26] where we need to understand the structures and properties of the epitaxial film or strained superlattice. The epitaxial Bain path, produced by isotropic stress or strain in the (100) plane of tetragonal phases accompanied by zero stress perpendicular to the plane, may help to predict which structure will form on a given substrate.

The martensitic transformation has a tie with both the phase stabilities and (the nonlinearity of) the elastic constants. Therefore, the calculation of the Bain path provides a comprehensive test for the validity of the present model. There are many paths to go from fcc to bcc or conversely. These paths are called Bain paths if the geometries along such a path have tetragonal symmetry. To calculate the Bain path means calculating the cohesive energy as a function of two lattice parameters a and c, $E(c,a)$, and finding the energy minimum for each given a, where a is the length of a face-centered orthorhombic cell in the x,y directions and c is that in the z direction. $c/a=1$ corresponds to the fcc structure while $c/a=\sqrt{2}/2$ corresponds to the bcc structure. The Bain paths for some transition metals including vanadium have been calculated by using the full-potential linearized augmented plane wave (FP-LAPW) method based on the density functional theory.[25] For vanadium, it is reported that for both the epitaxial Bain path (i.e., a is fixed and c adjusts to minimize the binding energy) and the uniaxial Bain path (i.e., c is fixed and a adjusts to minimize the binding energy) the fcc phase is a saddle point, while there exists a metastable body-centered-tetragonal (bct) phase. In Fig. 3 we show that the present model also predicts a similar epitaxial Bain path for vanadium, though the path shape and the magnitude of the energy difference are different. The saddle point predicted by the present model for vanadium (0.06 eV/atom) is about one-fifth of that by the *ab initio* method (0.29 eV/atom). The lattice constant and energy difference for the metastable bct phase given by the present model are $a=2.57$ Å ($c/a=1.67$) and 0.052 eV/atom, in comparison with the *ab initio* result $a=2.41$ Å ($c/a=1.83$) and 0.1 eV/atom. Although the potentials for Cr, Mo, and W present poor defect properties, the results for the elastic properties and phase stabilities are quite good; therefore we also calculate their Bain paths. For Nb, Cr, and W similar behaviors with that of V are found. But for Ta, Mo, and Fe, the Bain paths are found to have a plateau across the fcc phase. There is no metastable phase for these metals.

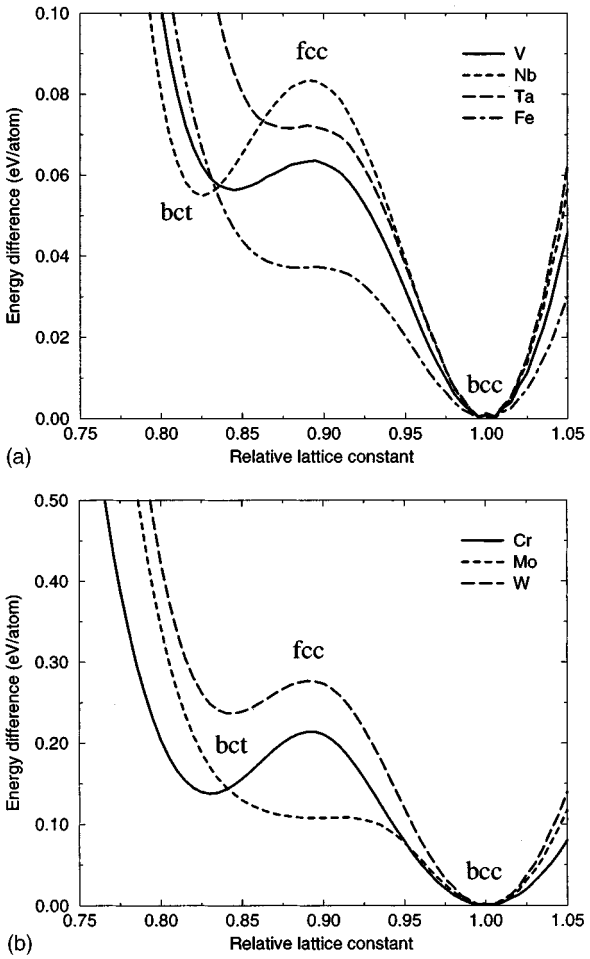

FIG. 3. Epitaxial Bain paths for the bcc transition metals. The relative lattice constant is defined as a/a_e, where a_e is the equilibrium lattice constant for the bcc structure. (a) V, Nb, Ta, and Fe; (b) Cr, Mo, and W.

VI. CONCLUDING REMARKS

Based on the perturbation method for the Hubbard model and the BOP, we have derived a semiempirical tight-binding model for the interatomic interaction. It is shown that the present model can be used to reproduce very well the elastic properties and phase stabilities of the bcc transition metals. However, the results of vacancy-formation energies and surface tensions for Cr, Mo, and W calculated with the suggested parameters are wrong.

Albeit the model is directly parametrized and used to simulate real metals, it does not necessarily mean that electron correlations are responsible for all the success and failure. The model just indicates the role of electron correlations on interatomic interaction and physical properties of materials with half-filled or nearly-half-filled bands.

ACKNOWLEDGMENTS

Q.X. would like to thank Professor David Pettifor for hospitality and discussion during his visit to the University of Oxford. He also gratefully acknowledges Professor Peter Fulde's helpful discussion and the hospitality of the Max-Planck-Institut für Physik komplexer Systeme.

APPENDIX

For cubic crystals, the formulas for $\delta C_{\mu\nu}$ and $\delta^2 C_{\mu\nu}$ can be written as

$$\Omega\,\delta C_{11}=U_1\left[\frac{1}{\Gamma}\frac{\partial^2 J}{\partial\varepsilon_{xx}^2}-\frac{J}{\Gamma^2}\frac{\partial^2\Gamma}{\partial\varepsilon_{xx}^2}-\frac{2}{\Gamma^2}\frac{\partial\Gamma}{\partial\varepsilon_{xx}}\frac{\partial J}{\partial\varepsilon_{xx}}+\frac{2J}{\Gamma^3}\left(\frac{\partial\Gamma}{\partial\varepsilon_{xx}}\right)^2\right], \tag{A1}$$

$$\Omega\,\delta C_{12}=U_1\left[\frac{1}{\Gamma}\frac{\partial^2 J}{\partial\varepsilon_{xx}\partial\varepsilon_{yy}}-\frac{J}{\Gamma^2}\frac{\partial^2\Gamma}{\partial\varepsilon_{xx}\partial\varepsilon_{yy}}-\frac{1}{\Gamma^2}\left(\frac{\partial\Gamma}{\partial\varepsilon_{xx}}\frac{\partial J}{\partial\varepsilon_{yy}}+\frac{\partial J}{\partial\varepsilon_{xx}}\frac{\partial\Gamma}{\partial\varepsilon_{yy}}\right)+\frac{2J}{\Gamma^3}\frac{\partial\Gamma}{\partial\varepsilon_{xx}}\frac{\partial\Gamma}{\partial\varepsilon_{yy}}\right], \tag{A2}$$

$$\Omega\,\delta C_{44}=U_1\left[\frac{1}{\Gamma}\frac{\partial^2 J}{\partial\varepsilon_{xy}^2}-\frac{J}{\Gamma^2}\frac{\partial^2\Gamma}{\partial\varepsilon_{xy}^2}\right] \tag{A3}$$

and

$$\Omega\,\delta^2 C_{11}=-U_2\left[\frac{1}{\Gamma^2}\frac{\partial^2 K}{\partial\varepsilon_{xx}^2}-\frac{2K}{\Gamma^3}\frac{\partial^2\Gamma}{\partial\varepsilon_{xx}^2}-\frac{4}{\Gamma^3}\frac{\partial\Gamma}{\partial\varepsilon_{xx}}\frac{\partial K}{\partial\varepsilon_{xx}}+\frac{6K}{\Gamma^4}\left(\frac{\partial\Gamma}{\partial\varepsilon_{xx}}\right)^2\right], \tag{A4}$$

$$\Omega\,\delta^2 C_{12}=-U_2\left[\frac{1}{\Gamma^2}\frac{\partial^2 K}{\partial\varepsilon_{xx}\partial\varepsilon_{yy}}-\frac{2K}{\Gamma^3}\frac{\partial^2\Gamma}{\partial\varepsilon_{xx}\partial\varepsilon_{yy}}-\frac{2}{\Gamma^3}\left(\frac{\partial\Gamma}{\partial\varepsilon_{xx}}\frac{\partial K}{\partial\varepsilon_{yy}}+\frac{\partial K}{\partial\varepsilon_{xx}}\frac{\partial\Gamma}{\partial\varepsilon_{yy}}\right)+\frac{6K}{\Gamma^4}\frac{\partial\Gamma}{\partial\varepsilon_{xx}}\frac{\partial\Gamma}{\partial\varepsilon_{yy}}\right], \tag{A5}$$

$$\Omega\,\delta^2 C_{44}=-U_2\left[\frac{1}{\Gamma^2}\frac{\partial^2 K}{\partial\varepsilon_{xy}^2}-\frac{2K}{\Gamma^3}\frac{\partial^2\Gamma}{\partial\varepsilon_{xy}^2}\right]. \tag{A6}$$

*Author to whom correspondence should be addressed.

[1] M. S. Daw and M. I. Baskes, Phys. Rev. Lett. **50**, 1285 (1983).
[2] F. Ercolessi, E. Tosatti, and M. Parrinello, Phys. Rev. Lett. **57**, 719 (1986).
[3] T. Tersoff, Phys. Rev. Lett. **56**, 632 (1986).
[4] D. G. Pettifor, Phys. Rev. Lett. **63**, 2480 (1989).
[5] M. Aoki, Phys. Rev. Lett. **71**, 3842 (1993).
[6] A. Horsfield *et al.*, Phys. Rev. B **53**, 1656 (1996).
[7] A. Horsfield *et al.* (unpublished).
[8] J. Friedel and C. M. Sayers, J. Phys. (France) **38**, 697 (1977).
[9] P. Fulde, *Electron Correlations in Molecules and Solids* (Springer, Berlin, 1995), Chap. 9.
[10] M. W. Finnis and J. F. Sinclair, Philos. Mag. A **50**, 45 (1984).
[11] D. Tomanek, A. A. Aligia, and C. A. Balseiro, Phys. Rev. B **32**, 5051 (1985).
[12] F. Cleri and V. Rosato, Phys. Rev. B **48**, 22 (1993).
[13] A. E. Carlsson, in *Solid State Physics*, edited by H. Ehrenreich and D. Turnbull (Academic, New York, 1990), Vol. 43.
[14] R. A. Johnson and D. J. Oh, J. Mater. Res. **4**, 1195 (1989).
[15] A. E. Carlsson, Phys. Rev. B **44**, 6590 (1991).
[16] For an excellent description, see M.C. Desjonqueres and D. Spanjaard, *Concepts in Surface Physics* (Springer, Berlin, 1993), Sec. 5.9.2.
[17] G. Simmons and H. Wang, *Single Crystal Elastic Constants and Calculated Aggregate Properties: A Handbook* (MIT Press, Cambridge, MA, 1971).
[18] Q. Xie and N. X. Chen, Phys. Rev. B **51**, 15 856 (1995).
[19] A. E. Carlsson, C. D. Gelatt, and H. Ehrenreich, Philos. Mag. A **41**, 241 (1980).
[20] M. Z. Bazant and E. Kaxiras, Phys. Rev. Lett. **77**, 4370 (1996).
[21] N. X. Chen, Phys. Rev. Lett. **64**, 1193 (1990).
[22] J. Maddox, Nature (London) **344**, 377 (1990).
[23] J. H. Rose, J. R. Smith, F. Guinea, and J. Ferrante, Phys. Rev. B **29**, 2963 (1984).
[24] C. Kittel, *Introduction to Solid State Physics*, 6th ed. (Wiley, New York, 1986).
[25] P. Alippi, P. M. Marcus, and M. Scheffler, Phys. Rev. Lett. **78**, 3892 (1997).
[26] E. Hahn, E. Kampshoff, N. Wälchli, and K. Kern, Phys. Rev. Lett. **74**, 1803 (1995).